J. Fluid Mech. (1991), *vol.* 231, *pp.* 35–50
Printed in Great Britain

Inviscid spatial stability of a three-dimensional compressible mixing layer

By C. E. GROSCH[1] AND T. L. JACKSON[2]

[1] Department of Oceanography and Department of Computer Science, Old Dominion University, Norfolk, VA 23529, USA

[2] Department of Mathematics and Statistics, Old Dominion University, Norfolk, VA 23529, USA

(Received 17 July 1990 and in revised form 28 February 1991)

We present the results of a study of the inviscid spatial stability of a parallel three-dimensional compressible mixing layer. The parameters of this study are the Mach number of the fast stream, the ratio of the speed of the slow stream to that of the fast stream, the ratio of the temperature of the slow stream to that of the fast stream, the direction of the crossflow in the fast stream, the frequency, and the direction of propagation of the disturbance wave. Stability characteristics of the flow as a function of these parameters are given. Certain theoretical results are presented which show the interrelations between these parameters and their effects on the stability characteristics. In particular, the three-dimensional stability problem for a three-dimensional mixing layer at Mach zero can be transformed to a two-dimensional stability problem for an equivalent two-dimensional mean flow. There exists a one-parameter family of curves such that for any given direction of mean flow and of wave propagation one can apply this transformation and obtain the growth rate from the universal curves. For supersonic convective Mach numbers, certain combinations of crossflow angle and propagation angle of the disturbance can increase the growth rates by a factor of about two, and thus enhance mixing.

1. Introduction

In recent years there has been renewed interest in understanding the stability characteristics of compressible mixing layers, due in part to the projected use of the scramjet engine for the propulsion of hypersonic aircraft. The study of the stability of these flows is particularly important because experimental and computational results show an increase in the flow stability at high Mach numbers. One effect of this is that the mixing between the fuel and oxidizer may decrease as the Mach number increases, resulting in partial burning and a loss in combustion efficiency. Because of this gain in stability, natural transition may occur at downstream distances which are larger than practical combustor lengths. Therefore, it is desirable to examine techniques which may enhance mixing. Knowledge of these characteristics may allow one, in principle, to control the downstream evolution of such flows. Further discussion of these issues and selected background for this problem were given in a recent paper by Jackson & Grosch (1989, hereinafter referred to as Part I).

All previous work on the stability of the compressible mixing layer are for two-dimensional mean flows. This is in contrast to the situation for boundary layers in which the effects of the crossflow on the stability have been studied and shown to be important (Mack 1984) in that it led to the appearance of standing wave instability

modes. There is no reason to believe that the effects of crossflow will not play an equally important role in determining stability characteristics of the compressible mixing layer. It is hoped that the inclusion of crossflow will enhance mixing, especially at supersonic speeds.

In Part I we presented comprehensive stability characteristics for a two-dimensional compressible mixing layer as a function of the parameters: the Mach number of the moving stream, the ratio of the temperature of the stationary stream to that of the moving stream, the frequency, and the direction of propagation of the disturbance wave. In a related study we examined the stability of a compressible mixing layer with an embedded flame sheet (Jackson & Grosch 1990*a*). The effects of thermodynamics of the mean flow on the flow stability have also been studied (Jackson & Grosch 1991). Finally we have also presented results relating to the transition from convective to absolute instability and a rigorous derivation of a convective Mach number for the two-dimensional compressible mixing layer (Jackson & Grosch 1990*b*).

In this paper we will examine the inviscid stability of a three-dimensional compressible mixing layer, the interfacial region between a fast moving gas at $+\infty$ and a slower moving gas at $-\infty$. In §2 we give the basic equations governing the three-dimensional mean flow. In §3 we formulate the stability problem, together with the boundary conditions and the numerical method of solution. Some general theoretical results are presented in §4. Section 5 contains a presentation of our numerical results and conclusions are given in §6.

2. Mean flow

We consider a three-dimensional compressible mixing layer, with zero pressure gradient, which separates two streams of different speeds and temperatures. We assume that the mean flow is governed by the three-dimensional compressible boundary-layer equations. We let (U, V, W) be the velocity components in the (x, y, z) directions, respectively, ρ the density, and T the temperature of this mean flow. All of the variables are non-dimensionalized using the magnitudes of the free-stream values at $y = +\infty$.

The mean flow equations are first transformed into the incompressible form by means of the Howarth–Dorodnitzyn transformation

$$Y = \int_0^y \rho \, \mathrm{d}y, \quad \hat{V} = \rho V + U \int_0^y \rho_x \, \mathrm{d}y, \tag{1}$$

yielding

$$\rho T = 1, \tag{2a}$$

$$U_x + \hat{V}_Y = 0, \tag{2b}$$

$$UU_x + \hat{V}U_Y = (\mu\rho U_Y)_Y, \tag{2c}$$

$$UW_x + \hat{V}W_Y = (\mu\rho W_Y)_Y, \tag{2d}$$

$$UT_x + \hat{V}T_Y = \left(\frac{\mu\rho}{\sigma} T_Y\right)_Y + (\gamma - 1) M^2 \mu\rho (U_Y^2 + W_Y^2), \tag{2e}$$

where μ is the coefficient of viscosity assumed to be only a function of temperature, σ the Prandtl number assumed to be constant, γ the ratio of specific heats, and M

the Mach number defined as the ratio of the speed of the fast moving stream to the speed of sound. Next we seek solutions in terms of the similarity variable

$$\eta = Y/(2x^{\frac{1}{2}}) \tag{3}$$

of the form

$$U = f'(\eta), \quad \hat{V} = (\eta f' - f)/x^{\frac{1}{2}}, \quad W = g(\eta), \quad T = T(\eta). \tag{4}$$

Substituting (4) into (2) yields the equations

$$\left(\frac{\mu}{T}f''\right)' + 2ff'' = 0, \tag{5a}$$

$$\left(\frac{\mu}{T}g'\right)' + 2fg' = 0, \tag{5b}$$

$$\left(\frac{\mu}{\sigma T}T'\right)' + 2fT' + (\gamma - 1)M^2\frac{\mu}{T}[(f'')^2 + (g')^2] = 0. \tag{5c}$$

Since the velocity components have been normalized by the speed of the fast stream, the appropriate boundary conditions are

$$U(\infty) = f'(\infty) = \cos\phi, \quad U(-\infty) = f'(-\infty) = \beta_U, \tag{6a}$$

$$W(\infty) = g(\infty) = \sin\phi, \quad W(-\infty) = g(-\infty) = 0, \tag{6b}$$

$$T(\infty) = 1, \quad T(-\infty) = \beta_T. \tag{6c}$$

Note that the fast stream is moving at an angle ϕ with respect to the x-axis, with $0° \leqslant \phi \leqslant 90°$. If $\phi = 0°$ there is no crossflow. If $\phi = 90°$ the flow at $+\infty$ is along the z-axis and at $-\infty$ is along the x-axis. The parameter β_U lies in the range $(0, \cos\phi)$. If β_T is less than 1, the slow stream is relatively cold compared to the fast stream, and if β_T is greater than 1 it is relatively hot.

Since the equation (5*b*) for g is linear, the solution is

$$g(\eta) = \frac{\sin\phi}{\cos\phi - \beta_U}(U - \beta_U). \tag{7}$$

Note that if $\beta_U = 0$, then g is proportional to U, and by an appropriate rotation of the axes, the mean flow can be reduced to a two-dimensional one, i.e. the angle ϕ can be scaled out of the problem. Thus we see that the parameter β_U plays an equivalent role to that of the pressure gradient parameter in a three-dimensional boundary-layer flow (Mack 1984).

The equations (5*a*, *c*) have a similarity solution. However, as discussed in Jackson & Grosch (1991), the qualitative stability characteristics are independent of the detailed shape of the mean profile. For this reason we assume here that

$$U = \tfrac{1}{2}(\cos\phi + \beta_U + (\cos\phi - \beta_U)\tanh\eta), \tag{8}$$

and thus from (7)

$$W = \tfrac{1}{2}\sin\phi(1 + \tanh\eta), \tag{9}$$

which approximates the similarity profiles and can be handled analytically. For Chapman's linear viscosity law and unit Prandtl number, the temperature is given by

$$T = 1 - (1 - \beta_T)\frac{\cos\phi - U}{\cos\phi - \beta_U} + \frac{\gamma - 1}{2}M^2\left[(\beta_U^2 - 1)\frac{\cos\phi - U}{\cos\phi - \beta_U} + 1 - U^2 - W^2\right]. \tag{10}$$

3. Stability problem

Following the formulation given in Jackson & Grosch (1989) and Lees & Lin (1946), the flow field is perturbed by introducing wave disturbances in the velocity, pressure, temperature and density with amplitudes which are functions of η. For example, the pressure perturbation is

$$p = \Pi(\eta) \exp[\mathrm{i}(\tilde{\alpha}x + \tilde{\beta}z - \omega t)], \tag{11}$$

with Π the amplitude, $\tilde{\alpha}$ and $\tilde{\beta}$ the wavenumbers in the downstream (x) and cross-stream (z) directions, respectively, and ω the frequency. Substituting the expression (11) for the pressure perturbation and similar expressions for the other flow quantities into the inviscid compressible equations yields the ordinary differential equations for the perturbation amplitudes. It is straightforward to derive a single equation governing Π, given by

$$\Pi'' - \frac{2(\tilde{\alpha}U' + \tilde{\beta}W')}{\tilde{\alpha}U + \tilde{\beta}W - \omega}\Pi' - T[(\tilde{\alpha}^2 + \tilde{\beta}^2)T - M^2(\tilde{\alpha}U + \tilde{\beta}W - \omega)^2]\Pi = 0, \tag{12}$$

where primes indicate differentiation with respect to the similarity variable η.

It is convenient to transform (12) to a form analogous to that for two-dimensional disturbances. To this end let

$$\tilde{\alpha} = \alpha\cos\theta, \quad \tilde{\beta} = \alpha\sin\theta, \tag{13}$$

with θ the angle of propagation of the disturbance wave with respect to the x-axis, and $-90° \leqslant \theta \leqslant 90°$. Applying this transformation to (12) yields

$$\Pi'' - \frac{2(U'\cos\theta + W'\sin\theta)}{U\cos\theta + W\sin\theta - c}\Pi' - T\alpha^2[T - M^2(U\cos\theta + W\sin\theta - c)^2]\Pi = 0, \tag{14}$$

where

$$c = \omega/\alpha. \tag{15}$$

If one considers spatial stability α is complex, with the real part of α being the wavenumber in the propagation direction and the imaginary part of α indicating whether the disturbance is amplified, neutral, or damped depending on whether α_{i} is negative, zero, or positive, assuming positive group velocity. The phase speed, c_{ph}, is given by $\omega/\alpha_{\mathrm{r}}$. If α_{i} is zero, $c = c_{\mathrm{N}}$ is the phase speed of a neutral mode. For temporal stability, α is real and ω is complex, and if the imaginary part of ω is positive the disturbances are amplified.

The boundary conditions for Π are obtained by considering the limiting form of (14) as $\eta \to \pm\infty$. The solutions to (14) are of the form

$$\Pi \to \exp(\pm\Omega_{\pm}\eta), \tag{16}$$

where

$$\Omega_+^2 = \alpha^2[1 - M^2(\cos(\phi - \theta) - c)^2], \quad \Omega_-^2 = \alpha^2\beta_T[\beta_T - M^2(\beta_U\cos\theta - c)^2]. \tag{17}$$

We define $c_{\pm}$ to be the values of the phase speed for which $\Omega_{\pm}^2$ vanishes. Thus

$$c_+ = \cos(\phi - \theta) - \frac{1}{M}, \quad c_- = \beta_U\cos\theta + \frac{\beta_T^{\frac{1}{2}}}{M}. \tag{18}$$

Note that c_+ is the phase speed of a sonic disturbance in the fast stream and c_- is the phase speed of a sonic disturbance in the slow stream. At

$$M = M_* \equiv \frac{1 + \beta_T^{\frac{1}{2}}}{\cos(\phi - \theta) - \beta_U\cos\theta} \tag{19}$$

$c_{\pm}$ are equal.

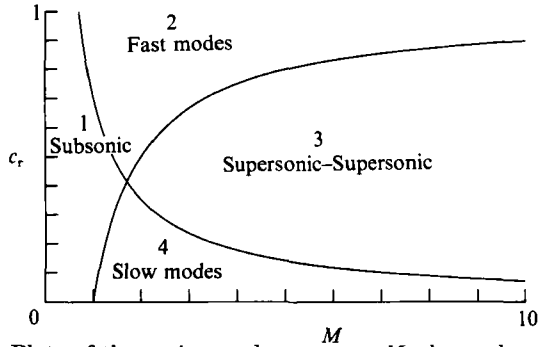

FIGURE 1. Plots of the sonic speeds $c_\pm$ versus Mach number for $\beta_T = 0.5$.

As discussed in Part I for a two-dimensional mean flow, the nature of the disturbances and the appropriate boundary conditions can now be illustrated by reference to figure 1, where we plot $c_\pm$ versus M for a typical value of β_T. These curves divide the (c_r, M) plane into four regions, where c_r is the real part of c. If a disturbance exists with a M and c_r in region 1, then Ω_+^2 and Ω_-^2 are both positive, and the disturbance is subsonic at both boundaries, and we classify it as a subsonic mode. In region 3, both Ω_+^2 and Ω_-^2 are negative and hence the disturbance is supersonic at both boundaries, and is classified as a supersonic–supersonic mode. In region 2, Ω_+^2 is positive and Ω_-^2 is negative, and the disturbance is subsonic at $+\infty$ and supersonic at $-\infty$, and we classify it as a fast mode. Finally, in region 4, Ω_+^2 is negative and Ω_-^2 is positive so that the disturbance is supersonic at $+\infty$ and subsonic at $-\infty$, and we classify it as a slow mode.

The appropriate boundary conditions for either damped or outgoing waves in the fast and slow streams are, respectively,

$$\Pi \to \exp(-\Omega_+ \eta) \quad \text{if} \quad c_r > c_+, \quad \Pi \to \exp[-i\eta(-\Omega_+^2)^{\frac{1}{2}}] \quad \text{if} \quad c_r < c_+, \tag{20a}$$

$$\Pi \to \exp(\Omega_- \eta) \quad \text{if} \quad c_r < c_-, \quad \Pi \to \exp[-i\eta(-\Omega_-^2)^{\frac{1}{2}}] \quad \text{if} \quad c_r > c_-. \tag{20b}$$

To solve the stability equation (14), we first transform it to a Riccati equation by setting

$$G = \Pi'/(\alpha T \Pi), \tag{21}$$

and then solve this new equation by the numerical scheme described in Part I, together with appropriate boundary conditions found from (20) and (21).

4. Theoretical results

In this section we present some theoretical results for a three-dimensional mean flow.

4.1. *Bounds on growth rates and phase speeds*

Rayleigh and Howard derived a number of theorems which provide bounds on the phase speed and/or growth rates of temporally growing disturbances in unstable, inviscid, incompressible shear flows (see Drazin & Reid 1984 for a comprehensive review). Chimonas (1970) extended the Rayleigh and Howard results to include compressibility. These results seem not to be well known, perhaps because Chimonas derived them in the context of meteorological problems. In a related study, Djordjevic & Redekopp (1988) derived similar results for a two-dimensional non-homentropic compressible flow.

We have extended Chimonas' results to include crossflow. These results only apply to temporally unstable flows. In addition, these results apply to subsonic or supersonic flows in a channel with boundaries at $\pm H$. They also apply to subsonic flows in an infinite domain for which the disturbances decay at $\pm\infty$. Following Chimonas' derivation, it is easy to show for temporal disturbances:

(*a*) that $(U\cos\theta + W\sin\theta - c_r)$ must change sign somewhere in the domain, i.e. that

$$c_r \in [(U\cos\theta + W\sin\theta)_{\min}, (U\cos\theta + W\sin\theta)_{\max}] = [\beta_U \cos\theta, \cos(\phi-\theta)], \tag{22}$$

where c_r is the phase speed of the temporally growing wave;

(*b*) that c_r, c_i lie within the semicircle

$$[c_r - \tfrac{1}{2}(\beta_U\cos\theta + \cos(\phi-\theta))]^2 + c_i^2 \leqslant [\tfrac{1}{2}(\cos(\phi-\theta) - \beta_U\cos\theta)]^2; \tag{23}$$

(*c*) and that the growth rate for the unstable modes satisfies

$$0 < \omega_i \leqslant \frac{(U'\cos\theta + W'\sin\theta)_{\max}}{2T_{\min}}, \tag{24}$$

when the variables are written in terms of the similarity variable η, with

$$T_{\min} = \min(1, \beta_T). \tag{25}$$

For the mean flow given by (8) and (9), the upper bound becomes

$$0 < \omega_i \leqslant \frac{\cos(\phi-\theta) - \beta_U\cos\theta}{4T_{\min}}. \tag{26}$$

Equation (22) extends Chimonas' result to include crossflow and shows that the phase speed of the unstable modes must lie in the range of the speed of the unperturbed free stream. Note that it is possible for these bounds to be equal. If the upper and lower bounds interchange, then the nominally slow stream now becomes the fast stream and this new problem can be transformed back into an equivalent problem. Equation (23) is exactly Chimonas' compressible semicircle theorem with crossflow. We see that it is possible for the radius of the semicircle to vanish, which then corresponds to a neutral mode. Equation (24) is Chimonas' upper bound with crossflow on the growth rate of the most unstable mode in a compressible flow. We see from (26) that the upper bound on the growth rate is proportional to the radius of the semicircle of (23), and both can vanish. These bounds may not be the best possible because they are independent of both the Mach number and the temperature distribution.

4.2. *Convective Mach number*

In a previous paper (Jackson & Grosch 1990*b*) we showed that for either a temporally or spatially unstable flow, a convective Mach number can be defined for a two-dimensional multi-species gas as

$$M_c = \frac{M}{M_*} \equiv \frac{M(1-\beta_U)\cos\theta}{1 + (\beta_\gamma/\beta_\rho)^{\frac{1}{2}}}, \tag{27}$$

where M is the Mach number of the fast stream, M_* is the Mach number at which the sonic speeds of the two streams are equal, β_ρ and β_γ are the ratios of density and specific heats, respectively, of the slow stream to that of the fast stream. In that paper we compared this definition of the convective Mach number to that proposed by others and to published experimental data. This definition of the convective Mach number with crossflow is based on the free-stream Mach number in the laboratory

frame and is independent of the speed of any large-scale structures. We also showed that $M = M_*$ ($M_c = 1$) is the largest Mach number for which any subsonic disturbances can exist. Finally, it was found that the maximum growth rates decreased as M_c approaches 1, while they level off for $M_c > 1$.

It is straightforward to generalize the above concept to a three-dimensional mean flow. For a single-species gas, using the definition of M_* from (19), we find

$$M_c = \frac{M}{M_*} \equiv \frac{M[\cos(\phi-\theta)-\beta_U\cos\theta]}{1+\beta_T^{\frac{1}{2}}}. \tag{28}$$

It is clear that (28) reduces to (27) if $\phi = 0°$ and $\beta_\gamma = 1$. If one is considering temporal instability, it can be seen that M_c is proportional to the radius of the semicircle (23) and also to the upper bound on the temporal growth rate (26). For a given value of M we can reduce M_c by decreasing the term in the square brackets in (28). However, trying to reduce M_c by doing this also reduces the radius of the semicircle and reduces the upper bound on the temporal growth rate. If the term in the square brackets in (28) is zero, the projection of the mean flow onto the direction of propagation is a constant, independent of η. Thus there is no effective shear, and thus no interaction between the mean flow and the disturbances.

4.3. *Generalized inflexion point*

Lees & Lin (1946) gave a necessary and sufficient condition for the existence of a neutral mode in region 1 of figure 1 for a two-dimensional mean flow. The corresponding result with crossflow is the condition

$$S(\eta) \equiv \frac{\mathrm{d}}{\mathrm{d}\eta}\left[\frac{U'\cos\theta+W'\sin\theta}{T^2}\right] = 0. \tag{29}$$

The real roots of S are the generalized inflexion points. Let η_c be such a root and define

$$\tilde{c} = U(\eta_c)\cos\theta + W(\eta_c)\sin\theta. \tag{30}$$

If $\tilde{c}$ lies in region 1 then, provided $\alpha \neq 0$, $\tilde{c} = c_N$ is the phase speed of a neutral mode. The corresponding neutral wavenumber, α_N, must be determined numerically. The eigenfunction is called a subsonic neutral mode. If $\tilde{c}$ lies in regions 2, 3, or 4, then it does not correspond to the phase speed of a neutral mode.

The function $S(\eta)$ is a cubic when U, W, and T are given by (8)–(10). Explicitly, (29) reduces to

$$(\cos(\phi-\theta)-\beta_U\cos\theta)(Z^3-aZ+b) = 0, \tag{31}$$

with

$$a = 1-\frac{4(1+\beta_T)}{(\gamma-1)M^2q^2}, \quad b = \frac{4(1-\beta_T)}{(\gamma-1)M^2q^2}, \tag{32}$$

where

$$Z \equiv \tanh\eta, \quad q^2 = 1-2\beta_U\cos\phi+\beta_U^2. \tag{33a, b}$$

Equation (31) has either one or three real roots with at least two of the three real roots equal if the discriminant is zero. If we define M_0 by

$$M_0 = \frac{2}{q(\gamma-1)^{\frac{1}{2}}}\{1+\beta_T+\tfrac{3}{2}(1-\beta_T)^{\frac{2}{3}}[(1+\beta_T^{\frac{1}{2}})^{\frac{2}{3}}+(1-\beta_T^{\frac{1}{2}})^{\frac{2}{3}}]\}^{\frac{1}{2}}, \tag{34}$$

then there is one real root for $M < M_0$ and three real roots for $M \geqslant M_0$. Note that M_0 increases as q decreases. In particular, as $M \to 0$, only one real root exists and is given by

$$Z = \frac{\beta_T-1}{\beta_T+1}, \tag{35}$$

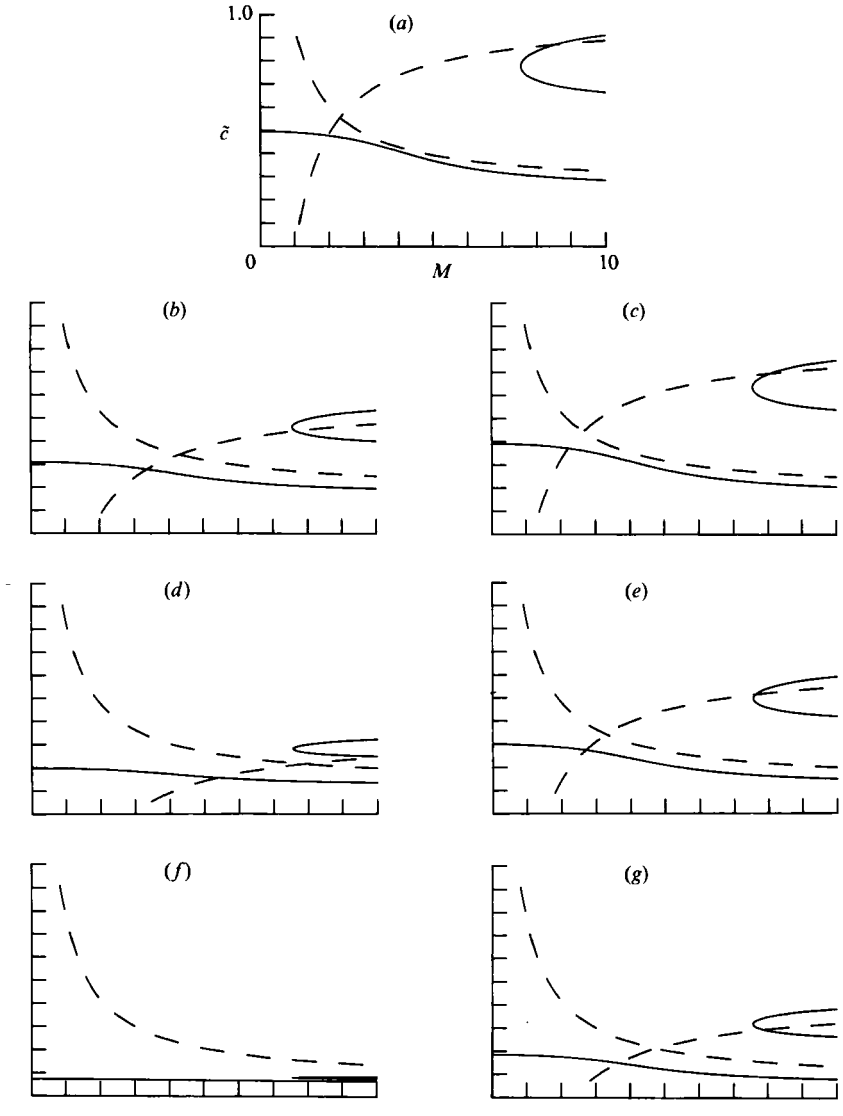

FIGURE 2. Plots of the real roots of S as a function of the Mach number for $\beta_T = \frac{1}{2}$, $\beta_U = 0.25$, $\phi = 10°$, and (a) $\theta = 0°$, (b) $\theta = -45°$, (c) $\theta = 45°$, (d) $\theta = -60°$, (e) $\theta = 60°$, (f) $\theta = -75°$, (g) $\theta = 75°$. Dashed lines show the sonic curves $c_{\pm}$.

with corresponding phase speed

$$c_N = \frac{\beta_T \cos(\phi - \theta) + \beta_U \cos\theta}{1 + \beta_T}. \tag{36}$$

Also, as $M \to \infty$, there are three real roots giving

$$\tilde{c} = \begin{cases} \frac{1}{2}[\cos(\phi - \theta) + \beta_U \cos\theta], & Z = 0, \\ \cos(\phi - \theta), & Z = 1, \\ \beta_U \cos\theta, & Z = -1. \end{cases} \tag{37}$$

Figure 2 is a plot of the real roots of S, $\tilde{c}$, from (31) as a function of the Mach number and for $\beta_T = \frac{1}{2}$, with $\beta_U = 0.25$, $\phi = 10°$, and various values of the

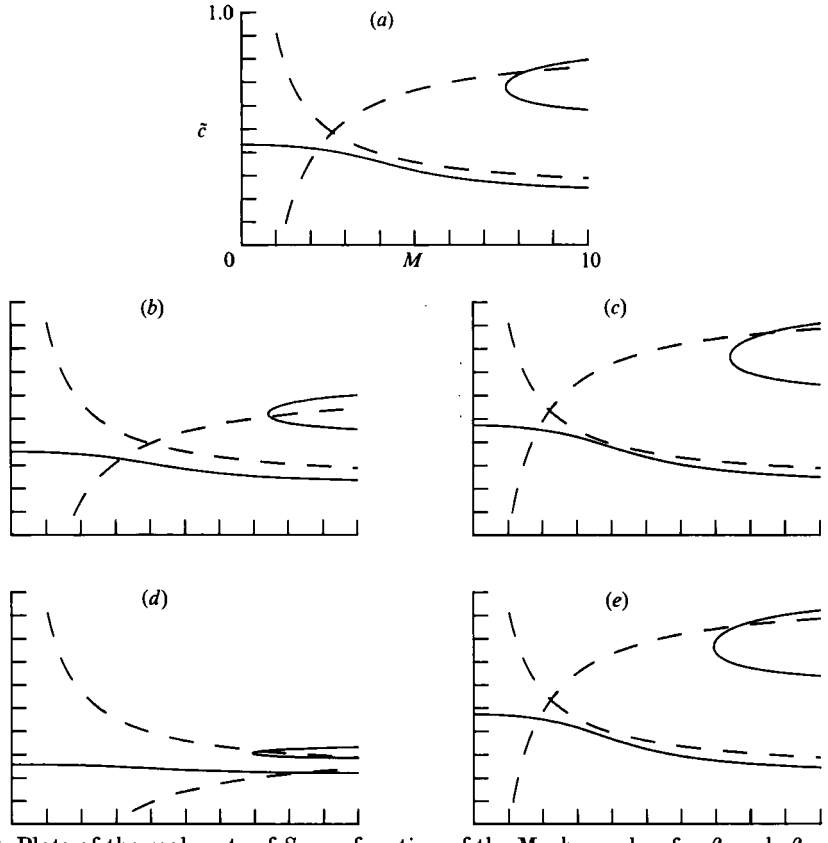

FIGURE 3. Plots of the real roots of S as a function of the Mach number for $\beta_T = \frac{1}{2}$, $\beta_U = 0.25$, (*a*) $\phi = 0°$ and $\theta = \pm 30°$, (*b*) $\phi = 20°$ and $\theta = -30°$, (*c*) $\phi = 20°$ and $\theta = 30°$, (*d*) $\phi = 40°$ and $\theta = -30°$, (*e*) $\phi = 40°$ and $\theta = 30°$. The sonic curves are plotted with dashes.

propagation angle θ. The sonic curves $c_\pm$ are also plotted with dashes. It should be remembered that it is only when $\tilde{c}$ lies in region 1 that it is the phase speed of a neutral mode. Figure 2 shows that the real zeros of S yield a monotonic curve and a 'bubble'. When $\beta_T < 1$, the monotonic curve decreases as the Mach number increases and moves from region 1 into region 4 and the 'bubble' lies above it. When $\beta_T > 1$, the monotonic curve increases as the Mach number increases and moves from region 1 into region 2 and the 'bubble' lies below it. When $\beta_T = 1$, the curve degenerates to a straight line and intersects the 'bubble'. Thus $\beta_T = 1$ is a transition value, denoted by $\hat{\beta}_T$. This unique value plays a critical role in the behaviour of the solutions of the stability problem (Jackson & Grosch 1991). As θ is either increased or decreased from 0°, the monotonic curves and the 'bubble' are shifted towards smaller values of $\tilde{c}$. It can be shown that the transition value $\hat{\beta}_T$ is independent of angle, although the corresponding value of $\tilde{c}$ is not. For any β_T, if the mode is two-dimensional ($\theta = 0°$) there is only one zero of S in region 1. However, the sonic speeds $c_\pm$ are functions of the angle of propagation. As θ increases or decreases from 0° the sonic curves shift towards higher Mach number.

To show the effect of direction of crossflow on the generalized inflexion points, we plot in figure 3 the real roots of S, $\tilde{c}$, from (31) as a function of the Mach number and for $\beta_T = \frac{1}{2}$, $\beta_U = 0.25$, $\theta = \pm 30°$, and for $\phi = 0°$, 20°, 40°. Again the sonic curves are plotted with dashes. For a disturbance propagating at a fixed angle of $\theta = 30°$,

increasing ϕ results in a small increase in the phase speed in region 1, while M_* decreases slightly. On the other hand, if $\theta = -30°$ increasing ϕ reduces the phase speed in region 1 and greatly increases the value of M_*. Therefore, the major effect on the phase speeds and M_* is observed when the disturbances are propagating in a direction opposite to that of the crossflow.

From the results shown above, one can conclude that for any value of β_T and ϕ, there will always be some angle of propagation for which all three zeros of S lie in region 1. Thus, the significance of the three real zeros of S only becomes apparent at large angles of propagation.

Finally, from (31) we see that another possible zero of S is given by the condition, $\cos(\phi-\theta)-\beta_U\cos\theta = 0$. However this condition implies that, for neutral disturbances, the radius of the semicircle (23), the upper bound on the temporal growth rate (26), and the convective Mach number (28) all vanish. This then corresponds to a neutral mode, with the projection of the mean flow onto the direction of propagation a constant.

5. Numerical results

In all of our calculations we have taken $\gamma = 1.4$ and $0 \leqslant M \leqslant 10$.

5.1. $M = 0$

Zero Mach number is a special case in that certain scalings are possible, because the viscous term in the temperature profile is absent. For zero Mach number, (14) reduces to

$$\Pi'' - \frac{2(U'\cos\theta + W'\sin\theta)}{U\cos\theta + W\sin\theta - c}\Pi' - \alpha^2 T^2 \Pi = 0, \tag{38}$$

with T given by (5c) or (10) with $M = 0$. Defining

$$\beta_U^* = \frac{\beta_U\cos\theta}{\cos(\phi-\theta)}, \quad c^* = \frac{c}{\cos(\phi-\theta)}, \quad \alpha^* = \alpha, \tag{39}$$

yields an equivalent disturbance equation

$$\Pi'' - \frac{2U^{*\prime}}{U^*-c^*}\Pi' - \alpha^{*2}T^{*2}\Pi = 0, \tag{40}$$

where

$$U^* = \frac{U\cos\theta + W\sin\theta}{\cos(\phi-\theta)}, \tag{41}$$

and

$$T^* = 1-(1-\beta_T)\frac{1-U^*}{1-\beta_U^*}, \tag{42}$$

for Chapman's viscosity law and unit Prandtl number, or an equivalent expression for the general case. With this scaling (40) is identical to (38) with $\phi = \theta = 0°$, and we see that the three-dimensional problem can be transformed to an equivalent two-dimensional problem. This is an extension of Squire's theorem to include a three-dimensional mean flow.

In order to illustrate the significance of the transformation (39), we show in figure 4 a plot of the maximum growth rate for $\phi = \theta = 0°$ and $\beta_T = \frac{1}{2}$, 1, 2 as a function

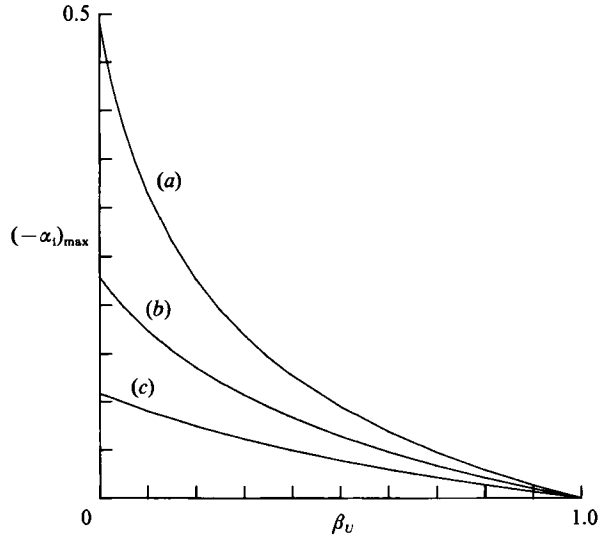

FIGURE 4. Plot of the maximum growth rate versus β_U for $M = 0$, $\phi = \theta = 0°$, and (*a*) $\beta_T = \frac{1}{2}$, (*b*) $\beta_T = 1$, (*c*) $\beta_T = 2$.

of β_U. The graph for $\beta_T = 1$ is equivalent to that of Monkewitz & Huerre (1982). We note that as ϕ and θ are varied, the only result is that the curves of figure 4 are shifted to the right or to the left. In particular, if $\phi = 0°$ then $\beta_U^* = \beta_U$ for any θ and the growth rate at Mach zero is that given in figure 4. Next, if ϕ is not zero but fixed, there are three cases:

(i) if $\theta = \frac{1}{2}\phi$, then $\beta_U^* = \beta_U$ and again the growth rate is that of figure 4;

(ii) if $\theta > \frac{1}{2}\phi$, then $\beta_U^* < \beta_U$ and is shifted towards zero as θ increases, and therefore the maximum growth rate is increased;

(iii) if $\theta < \frac{1}{2}\phi$, then $\beta_U^* > \beta_U$ and is shifted towards 1 as θ decreases, and therefore the maximum growth rate is decreased.

Thus for a given β_T and β_U, one can predict how a variation in ϕ and θ will affect the maximum growth rate at zero Mach number. This also has significance for the maximum growth rates for $M > 0$ as will be shown in §5.3.

Finally, based on our numerical results, we find that for $M = 0$,

$$c_N = \frac{\beta_T \cos(\phi-\theta) + \beta_U \cos\theta}{1+\beta_T}, \quad \alpha_N = \frac{1+\beta_T}{2\beta_T}, \quad \omega_N = \frac{\beta_T \cos(\phi-\theta) + \beta_U \cos\theta}{2\beta_T}. \tag{43}$$

5.2. *Absolute/convective instabilities*

A flow is said to be absolutely unstable if the response to an impulse in space and time is unbounded everywhere in space for large time. A flow is said to be convectively unstable if the response decays to zero everywhere in space for large enough time. In this latter case the response to the impulse is a wave packet propagating downstream from the source with the waves forming the packet having growing amplitudes. Recently, Pavithran & Redekopp (1989) and Jackson & Grosch (1990*b*) have studied the transition from convective to absolute instability in a compressible, subsonic, two-dimensional mixing layer. At zero Mach number and $\beta_T = 1$, the transition value of β_U is -0.136, corresponding to backflow. For β_U greater than this value the flow is convectively unstable, while for values less than this it is absolutely unstable. An increase in β_T from 1 causes the transition value of β_U to become more negative,

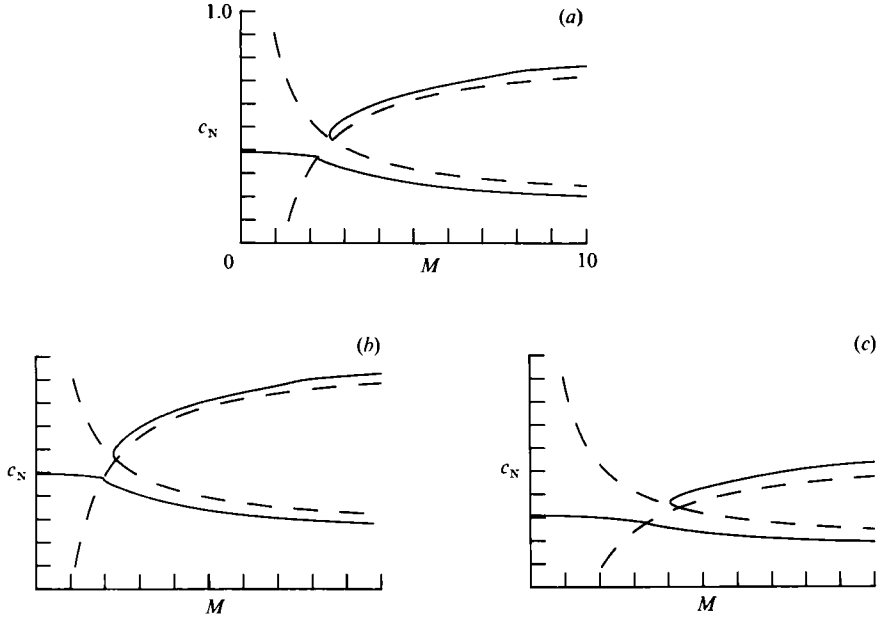

FIGURE 5. Plots of the neutral phase speeds versus Mach number for $\beta_T = \frac{1}{2}$, $\beta_U = 0.25$, $\phi = 10°$, and (a) $\theta = 45°$, (b) $\theta = 0°$, (c) $\theta = -45°$. The sonic curves $c_\pm$ are shown as dashed curves.

while decreasing β_T from 1 has the opposite effect (Jackson & Grosch, 1990*b*), but even for small β_T the transition value is still negative. For any value of β_T, increasing the Mach number causes the transition value of β_U to become more negative. Thus, the two-dimensional mixing layer is convectively unstable.

We have extended these results to include crossflow. In particular, at zero Mach number we can use the transformations (39) to determine the transition value of β_U for any set of values of ϕ and θ from the β_U of the equivalent two-dimensional mean flow. Because these two values of β_U are related by cosine factors, the signs never change. Hence, the compressible, subsonic, three-dimensional mixing layer is also convectively unstable.

5.3. $M > 0$

For Mach numbers greater than zero it is not possible to scale the mean flow to reduce it to an equivalent two-dimensional mean flow. In what follows we have taken $\beta_T = \frac{1}{2}$ because cooling the gas of the slow stream results in an increase in the maximum growth rates of the disturbances. In addition we also take $\beta_U = 0.25$.

Results for the neutral modes are shown in figure 5 for $\phi = 10°$ and $\theta = -45°$, 0°, 45°. Figure 5 shows the variation of the phase speed c_N as a function of the Mach number. Note that as θ is decreased there is a substantial increase in the extent of region 1. As in Part I, there is a single subsonic neutral wave in region 1 which crosses over the sonic curve at M_s, the Mach number at which the phase speed equals that of a sonic wave, into region 4 and is transformed into a slow supersonic neutral mode. There is also another supersonic neutral mode which appears at M_* in region 2 and is classified as a fast supersonic neutral mode.

In figures 6, 7, and 8 we show the variation of maximum value of growth rate with Mach number for selected values of ϕ and θ. In figure 6, ϕ is taken to be 10° and maximum growth rates are given for several values of θ. A decrease in θ from 80° results in a decrease in the maximum value of the growth rate for low Mach numbers.

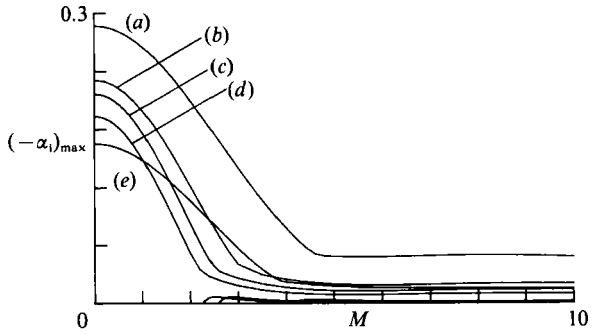

FIGURE 6. Plot of the maximum growth rates of the subsonic modes and their slow supersonic continuation and some fast supersonic modes versus Mach number for $\beta_T = \frac{1}{2}$, $\beta_U = 0.25$, $\phi = 10°$, and (*a*) $\theta = 80°$, (*b*) $\theta = 60°$, (*c*) $\theta = 45°$, (*d*) $\theta = 0°$, (*e*) $\theta = -45°$.

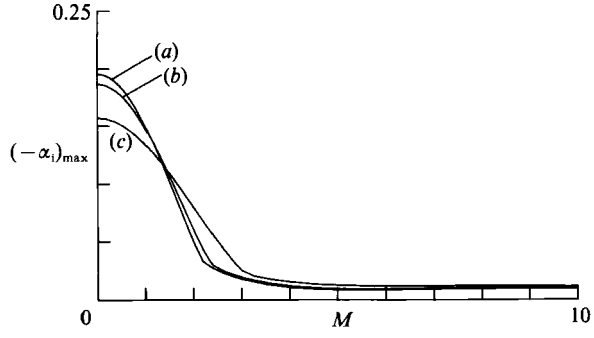

FIGURE 7. Plot of the maximum growth rates of the subsonic modes and their slow supersonic continuation versus Mach number for $\beta_T = \frac{1}{2}$, $\beta_U = 0.25$, $\theta = 0°$, and (*a*) $\phi = 0°$, (*b*) $\phi = 20°$, (*c*) $\phi = 40°$.

In particular the results at Mach zero are a consequence of the transformations given in §5.1. As θ decreases towards and past $\frac{1}{2}\phi$, β_U^* shifts away from zero and therefore the maximum growth rate decreases. For all values of θ the trend in the maximum growth rate with Mach number is similar. For the subsonic mode and its slow supersonic continuation the growth rates decrease by a factor of five to ten with Mach number and then level off. The growth rates of the fast supersonic modes, which appear at M_*, increase slightly and then decrease with increasing Mach number. Since the growth rates of these modes are always considerably less than those of the others, we do not show them in figures 7 and 8. Note that the growth rate for $\theta = 80°$ is always greater than the growth rates of the other cases. At Mach two, the growth rate of the $\theta = 80°$ case is comparable to the growth rate of the $\theta = 0°$ case at Mach zero.

Figure 7 shows the growth rates for a complementary case; θ held fixed at 0° and $\phi = 0°, 20°, 40°$. An increase in ϕ results in a decrease in the growth rates at low Mach numbers. As in the previous case, an increase in Mach number causes first a decrease in the growth rate, followed by a levelling off for all angles. Note from the transformation (39), with two-dimensional disturbances ($\theta = 0°$) and zero Mach number, $\beta_U^* = \beta_U/\cos\phi$. Thus as ϕ is increased from zero, β_U^* increases and hence the maximum growth rate decreases. This behaviour influences the growth rates at low subsonic Mach numbers. Therefore, to take advantage of the effects of crossflow, one must also have three-dimensional disturbances.

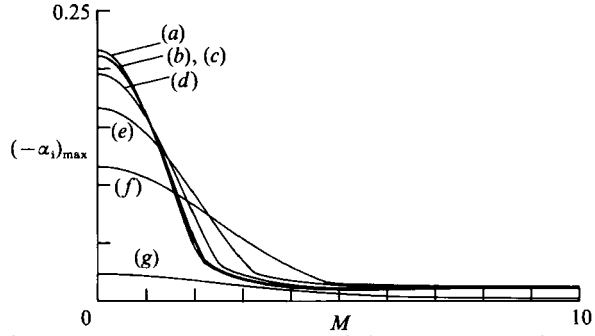

FIGURE 8. Plot of the maximum growth rates of the subsonic modes and their slow supersonic continuation versus Mach number for $\beta_T = \frac{1}{2}$, $\beta_U = 0.25$, and (*a*) $\phi = 30°$ and $\theta = 30°$, (*b*) $\phi = 15°$ and $\theta = 30°$, (*c*) $\phi = 45°$ and $\theta = 30°$, (*d*) $\phi = 0°$ and $\theta = \pm 30°$, (*e*) $\phi = 15°$ and $\theta = -30°$, (*f*) $\phi = 30°$ and $\theta = -30°$, (*g*) $\phi = 45°$ and $\theta = -30°$.

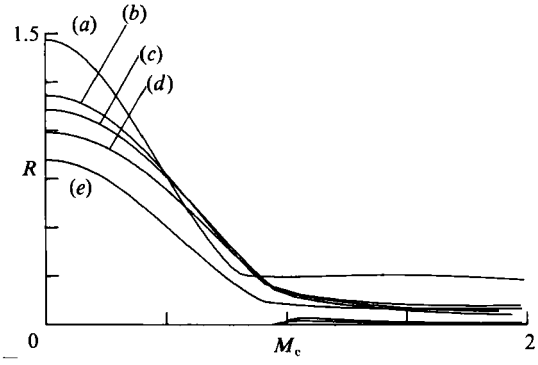

FIGURE 9. Plot of the normalized maximum growth rate as a function of the convective Mach number for $\beta_T = \frac{1}{2}$, $\beta_U = 0.25$, $\phi = 10°$, and (*a*) $\theta = 80°$, (*b*) $\theta = 60°$, (*c*) $\theta = 45°$, (*d*) $\theta = 0°$, (*e*) $\theta = -45°$.

The results in figure 8 are intended to show the effect on the growth rate of modes propagating in the direction of the crossflow and counter to the crossflow. To do this we have chosen two values of propagation, $\theta = \pm 30°$ and four values of ϕ. At zero Mach number the case of $\phi = \theta = 30°$ has the maximum growth rate, while the case $\phi = 45°$ and $\theta = -30°$ has the minimum. But at higher Mach numbers, say greater than Mach 2.5, the case with $\phi = 30°$ and $\theta = -30°$ has the largest growth rate. All of the growth rates at Mach zero can be found using the transformation (39) and the results shown in figure 4.

The effect on the growth rates of the scaling parameter M_c defined in (28) can now be analysed. In order to show the variation of the maximum growth rates with M_c we define the normalized growth rate

$$R = \frac{(-\alpha_i)_{max}(\beta_U, \beta_T, M, \phi, \theta)}{(-\alpha_i)_{max}(\beta_U, \beta_T, 0, 0, 0)}. \tag{44}$$

Figure 9 is a plot of the normalized growth rate R versus the convective Mach number M_c of the data shown in figure 6. In all cases the normalized growth rate decreases by a factor of five to ten as the convective Mach number increases from zero to one. For $M_c > 1$, corresponding to the slow supersonic continuation of the subsonic mode in region 1 into region 4 (see figure 1), the normalized growth rates level off. In addition, the fast supersonic modes in region 2 of figure 1 appear. Finally,

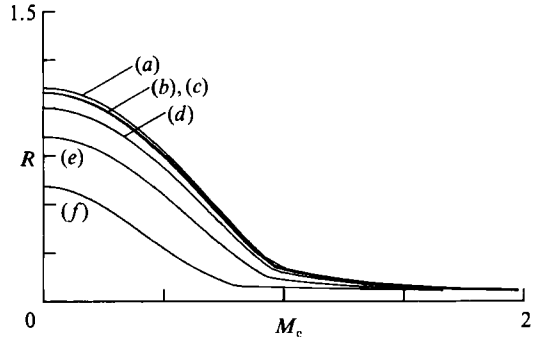

FIGURE 10. Plot of the normalized maximum growth rate as a function of the convective Mach number for $\beta_T = \frac{1}{2}$, $\beta_U = 0.25$, and (*a*) $\phi = 30°$ and $\theta = 30°$, (*b*) $\phi = 15°$ and $\theta = 30°$, (*c*) $\phi = 45°$ and $\theta = 30°$, (*d*) $\phi = 0°$ and $\theta = \pm 30°$, (*e*) $\phi = 15°$ and $\theta = -30°$, (*f*) $\phi = 30°$ and $\theta = -30°$.

for $M_c > 1$, the growth rate of the $\theta = 80°$ case is substantially larger than the growth rates of the other cases. Figure 10 shows similar trends in the growth rates for the data shown in figure 7.

7. Conclusions

We have presented theoretical bounds on the phase speeds and growth rates for temporally growing disturbances in a three-dimensional compressible mixing layer. We also derived a convective Mach number appropriate for either temporal or spatial instabilities. For temporal instabilities, it was found that the convective Mach number is proportional to these bounds. In order to enhance mixing, it is generally desirable to decrease the convective Mach number so as to have higher growth rates. However, we have shown that decreasing the convective Mach number also decreases the bounds on the growth rates.

For Mach zero we have shown that the three-dimensional stability problem for a three-dimensional mixing layer can be transformed to a two-dimensional stability problem for an equivalent two-dimensional mean flow. There exists a one-parameter family of curves, with β_T the parameter, of the maximum growth rate as a function of β_U. For any given direction of flow and of wave propagation one can apply the transformation and obtain the growth rate from the universal curves. In addition, we have shown that the subsonic three-dimensional mixing layer is convectively unstable.

For spatial instability and convective Mach numbers greater than zero, maximum growth rates always decrease by a factor of five to ten as the convective Mach number approaches 1. The maximum growth rates level off for convective Mach numbers greater than 1. However, for a modest crossflow angle and large positive angle of propagation, it is possible to increase the growth rate beyond $M_c = 1$ relative to the two-dimensional case. This effect is significant since growth rates can be increased by a factor of about two in the range of convective Mach numbers greater than 1. However, this is not enough to increase the growth rates of these modes to those of the subsonic modes at Mach zero. We conclude that crossflow can increase the mixing and thus enhance combustion efficiency at supersonic convective Mach numbers. We suggest that a pressure gradient or streamwise vorticity may also contribute to a further destabilization of these modes.

We wish to thank D. Bushnell for suggesting that we examine this problem.

REFERENCES

CHIMONAS, G. 1970 The extension of the Miles–Howard theorem to compressible fluids. *J. Fluid Mech.* **43**, 833–836.

DJORDJEVIC, V. D. & REDEKOPP, L. G. 1988 Linear stability analysis of nonhomentropic, inviscid compressible flows. *Phys. Fluids* **31**, 3239–3245.

DRAZIN, P. G. & REID, W. H. 1984 *Hydrodynamic Stability*. Cambridge University Press.

JACKSON, T. L. & GROSCH, C. E. 1989 Inviscid spatial stability of a compressible mixing layer. *J. Fluid Mech.* **208**, 609–637 (referred to herein as Part I).

JACKSON, T. L. & GROSCH, C. E. 1990*a* Inviscid spatial stability of a compressible mixing layer. Part 2. The flame sheet model. *J. Fluid Mech.* **217**, 391–420.

JACKSON, T. L. & GROSCH, C. E. 1990*b* Absolute/convective instabilities and the convective Mach number in a compressible mixing layer. *Phys. Fluids* A **2**, 949–954.

JACKSON, T. L. & GROSCH, C. E. 1991 Inviscid spatial stability of a compressible mixing layer. Part 3. Effects of thermodynamics. *J. Fluid Mech.* **224**, 159–175.

LEES, L. & LIN, C. C. 1946 Investigation of the stability of the laminar boundary layer in a compressible fluid. *NACA TN* 1115.

MACK, L. M. 1984 Boundary layer linear stability theory. In *Special Course on Stability and Transition of Laminar Flow, AGARD Rep.* **R-709**, pp. 3-1 to 3-81.

MONKEWITZ, P. A. & HUERRE, P. 1982 Influence of the velocity ratio on the spatial instability of mixing layers. *Phys. Fluids* **25**, 1137–1143.

PAVITHRAN, S. & REDEKOPP, L. G. 1989 The absolute-convective transition in subsonic mixing layers. *Phys. Fluids* A **1**, 1736–1739.